Query Details Back to Main Page

1. Journal instruction requires a city and country for affiliations; however, these are missing in affiliation [1, 2]. Please verify if the provided city and country are correct and amend if necessary.

Yes correct. We just modified "Turin" in "Torino", thanks.

2. Figure [6] was received; however, no citation was provided in the manuscript. Please check and confirm the inserted citation of Fig/Table is correct. If not, please suggest an alternative citation. Please note that figures and tables should be cited in ascending numerical order in the text. and should be inside the main body of the text.

We added the citation of Figure 6 in the text (just before the citation of Figure 7)

3. Equation: As per journal standards, the numbering of equations should be in ascending numerical order; hence, equations and eqs citations were renumbered accordingly. Please check if action is appropriate.

We modified some references, thank you.

4. Kindly check and confirm tha affiliations are processed correctly.

Yes, thanks.

5. Kindly provide complete details for reference [31].

Cattari et al. (2019a) Discussion on data recorded by the Italian structural seismic monitoring network on three masonry structures hit by the 2016-2017 Central Italy earthquake, in Proc. COMPDYN 2019, Crete, Greece, 24-26 June 2019

Seismic damage identification by fitting the nonlinear and hysteretic dynamic response of monitored buildings

Gaetano Miraglia, [1,2]

Erica Lenticchia, [1,2]

Cecilia Surace, [1,2]

Rosario Ceravolo, [1✉,2]

Email rosario.ceravolo@polito.it

[1] Department of Structural, Geotechnical and Building Engineering, DISEG, Politecnico di Torino, Torino, Italy

[2] Responsible Risk Resilience interdepartmental Centre (R3C), Politecnico di Torino, Torino, Italy

Received: 19 November 2019 / Accepted: 20 March 2020

Abstract

The identification of hysteretic degrading systems exposed to nonstationary loading is a paramount research topic, especially in the case of structures subjected to ground motion excitations. In this paper, the data recorded by a masonry building are used to detect the presence of seismic damage. To this aim, a parametric nonlinear identification is performed by adopting a Bouc–Wen-type multiple oscillator model. Starting from the results of the identification process, a damage index based on the degrading stiffness matrix is defined. The damage index provides preliminary information to be used in post-event management. Finally, the identification procedure is applied to a monitored masonry structure, the Town Hall of Pizzoli (L'Aquila), which is part of the Italian Seismic Observatory of Structures (OSS). The records measured by accelerometers permanently installed on the building are used for the detection of damage occurred during a seismic event.

Keywords

Seismic damage
Nonlinear response
Structural Health Monitoring
Hysteretic system identification
Post-event management

1. Introduction

The identification of hysteretic degrading systems subject to nonstationary excitation is becoming an important research topic, especially when studying the seismic response of structures subjected to ground motion excitation [1, 2, 3]. Not only is the seismic response of a building a typically transient and nonstationary phenomenon, but it is also associated to a progressive deviation of the system's structural parameters. Thus, the importance of this research lies in

the fact that nonlinearity needs to be identified and separated from non-stationarity. In addition, information extracted from nonlinear identification techniques can be used to define damage indicesexes [4], which in turn are of great help to manage decision-making process after seismic events [5].

AQ1

Indeed, in the phases immediately following a seismic event, one of the problems to be faced is that of a rapid, accurate and reliable assessment of the damages [6], which is useful for the coordination of immediate interventions for securing and/or clearing potentially damaged buildings [7]. Integrating damage indicesexes into a decision-making and alert system can be of considerable help in these circumstances allowing the identification of the most damaged structures in real time, and therefore, the definition of a hierarchy to follow in the management of emergency interventions.

The damage can be defined as a change introduced in a system that negatively affects its current and future performance [8]. Structural Health Monitoring (SHM) techniques are precisely intended to provide some physical based damage indicesexes with a broad range of validity, in linear and nonlinear field. Usually, a nonlinear hysteretic behaviour, with or without degradation, is associated with permanent change in the structure and, correspondingly, local plasticization of materials will inevitably affect their future performances.

Among several models that can be used to simulate hysteretic systems, the Bouc–Wen (BW)-type models, e.g. [9, 10]. and [11], have proved to be very flexible, even though a range of validity for both the model parameters and the input signals exists [12]. The identification methods for nonlinear systems are usually classified in two families: (i) parametric [13, 14, 15], and (ii) non-parametric methods [16, 17, 18]. Recently, new nonlinear identification methods were introduced that extract governing equation via sparse regression, offering a physical insight to non-parametric approaches [19, 20].

As regards to parametric identification , some recent works [21] analysed, the experimental dynamical response of three types of nonlinear hysteretic systems by employing phenomenological models together with the differential evolutionary algorithm.

Another important classification of the identification methods for nonlinear systems is based on the domain in which the identification is performed: frequency, time, or joint time–frequency domain, e.g. [22, 23]. The idea underlying time–frequency identification techniques is that, for certain classes of structural response signals, the limited availability of experimental data can be

partially obviated by taking into account the localization in time of the frequency components of the signals, see for example, the work of [23] and [24].

Time–frequency identification techniques, in particular, are useful to perform instantaneous identifications of structural features [2, 25]. Instantaneous estimates of model parameters can also be obtained with tools such as the Unscented Kalman Filter (UKF), which has been ~~also~~ proposed for the real-time identification of multi-storey buildings, e.g. [26].

The main object of the present paper is a procedure to perform an instantaneous hysteretic identification of chain-like Multi Degree of Freedom (MDoF) systems for the detection of seismic damage. An inter-story Bouc–Wen hysteretic model with degradation is used to capture the real-time dynamic behaviour of a masonry building affected by strong seismic events. The importance of the work also lies in the ability of the method to supply information on the damage accumulated by monitored buildings.

In more details, Sect. 2 introduces the method. In Sect. 3, the procedure to identify the seismic damage is applied to a reduced 2 DoF model of a monitored building, while the verification of the methods on the real structure is reported in Sect. 4. Finally, conclusions are drawn in Sect. 5.

2. Methods

In this section, the methodology methods used for the nonlinear identification of the seismic damage in lumped mass MDoF systems is discussed. Bold italic is herein used for vectors and bold capital for matrices. We assume to approximate the experimental record, ${}^{d}n_e(t)$, of a general Degree of Freedom (DoF) d with the following generalized linear expansion form:

$$ {}^{d}n_n(t) = \sum_{i=1}^{{}^{d}I} {}^{d}p_i \bullet {}^{d}n_i(t) \cong {}^{d}n_e(t) \tag{1} $$

where ${}^{d}n_n(t)$, is the numerical approximation of the records, ${}^{d}p_i$ are the system parameters to be identified, ${}^{d}n_i(t)$, are the basis functions and ${}^{d}I$ is the total number of basis functions used to approximate the d-th experimental record, while t denotes the time. Equation (1), likewise in [16], represents a generalized linear expansion of the experimental records.

The first goal of this section is to find the parameters, ${}^{d}p_i$, for a general DoF using a linear Time–Frequency Distribution (TFD) operator, $T(\bullet)$, allowing the

instantaneous estimation of the parameters of the model. For this reason, we rewrite (1) as:

$$ {}^{d}W(f,t;{}^{d}\boldsymbol{p}) = \| T\left({}^{d}n_n(t)\right) - T\left({}^{d}n_e(t)\right) \|_2^2 = \| T\left({}^{d}n_n(t) - {}^{d}n_e(t)\right) \|_2^2 \qquad 2 $$

where ${}^{d}W(f,t;{}^{d}\boldsymbol{p})$ is the norm-2 squared of the TFD of the errors that need to be minimized. For this purpose, we define the following quantities, for i and k that go from 1 to ${}^{d}I$ with step 1:

$$ {}^{d}Q_{ik} = {}^{d}Q_{ik}\left(f,t;{}^{d}\boldsymbol{p}\right) = T_{Re}\left({}^{d}n_i\right) \bullet T_{Re}\left({}^{d}n_k\right) + T_{Im}\left({}^{d}n_i\right) \bullet T_{Im}\left({}^{d}n_k\right) \qquad 3 $$

$$ {}^{d}Q_{ie} = {}^{d}Q_{ie}(f,t;{}^{d}\boldsymbol{p}) = T_{Re}\left({}^{d}n_i\right) \bullet T_{Re}\left({}^{d}n_e\right) + T_{Im}\left({}^{d}n_i\right) \bullet T_{Im}\left({}^{d}n_e\right) \qquad 4 $$

where the operators $T_{Re}(\bullet)$, $T_{Im}(\bullet)$ define the real and imaginary part of the TFD of the quantity contained in $(\bullet)$. The parameters ${}^{d}p_i$, can then be estimated by solving the following problem:

$$ \begin{cases} {}_{o}{}^{d}\boldsymbol{p} = {}^{d}\mathbf{H}^{-1}\,{}^{d}\boldsymbol{b}, \forall t \\ {}^{d}H_{ik}(t) = 2\int_0^t \left(\int_0^{f_s/2} {}^{d}Q_{ik}(f,\tau;{}^{d}\boldsymbol{p})df \right) d\tau \\ {}^{d}b_i(t) = 2\int_0^t \left(\int_0^{f_s/2} {}^{d}Q_{ie}(f,\tau;{}^{d}\boldsymbol{p})df \right) d\tau \end{cases} \qquad 5 $$

where f_s is the sampling frequency of the signal ${}^{d}n_e(t)$. If the integrals $\int_0^t (\bullet)\, d\tau$ in (5) are computed for $t = t_e$, where t_e is the time-length of the signal, it is possible to get a unique value scalar estimate of ${}_{o}{}^{d}\boldsymbol{p}$ in the time, i.e. the parameters that minimize (2). Then, if the restoring force is approximated with a simple Bouc–Wen oscillator with stiffness proportional to the dissipated energy and without viscous term, (6), (7), (8) (8) and (9) provide the form of ${}^{d}p_i$, ${}^{d}n_i(t)$ and ${}^{d}n_e(t)$ with the following assumptions: $\dot{u}_0 = 0$, $f_{D+1,NL}(t) = 0$ and $f_{D,KL}(t) = 0$, with D total number of DoFs; $f_{d,KL}(t)$ is a known function that depends only on the symmetric parameter and functions already found (i.e. $K_{0,rd} = K_{0,dr}$, $\varepsilon_{rd}(t) = -\varepsilon_{dr}(t)$, $\delta_{rd} = -\delta_{dr}$, $\forall r \neq d$).

6

$$ {}^{d}p_i \begin{cases} if, 1 \le i \le D \forall i \in N \\ K_{0,dr} \forall r, \\ \\ if, (D+1) \le i \le 2D \forall i \in N \\ K_{0,dr} \delta_{dr} \forall r, \\ \\ if, i = 2D+1 \\ \beta_d, \\ \\ if, i = 2D+2 \\ \gamma_d, \end{cases} $$

$$ {}^{d}n_i\left(t\right) \begin{cases} if, 1 \le i \le D \forall i \in N \\ \frac{u_r(t)}{m_d} \forall r, \\ \\ if, (D+1) \le i \le 2D \forall i \in N \\ \int_0^t -\left(\frac{\varepsilon_{dr}(\tau)\dot{u}_r(\tau)}{m_d}\right) d\tau \forall r, \\ \\ if, i = 2D+1 \\ {}^{d}n_{2D+1}\left(t\right), \\ \\ if, i = 2D+2 \\ \int_0^t \left(\frac{(\dot{u}_{d-1}(\tau)-\dot{u}_d(\tau))}{m_d} \left|\sum_{r=D}^{d} f_d\left(\tau\right)\right|^{N_d}\right) d\tau, \end{cases} \quad (7) $$

$$ {}^{d}n_{2D+1}\left(t\right) = \int_0^t \left(\frac{(\dot{u}_{d-1}(\tau)-\dot{u}_d(\tau))}{m_d} \left|\sum_{r=D}^{d} f_d\left(\tau\right)\right|^{N_d} \bullet sign\left[\left(\dot{u}_d\left(\tau\right) - \dot{u}_{d-1}\left(\tau\right)\right) \sum_{r=D}^{d} f_d \right. \right. $$

$$ {}^{d}n_e\left(t\right) = -\left(a\left(t\right) + \ddot{u}_d\left(t\right)\right) + \frac{\sum_{z=d}^{D} f_{z+1,NL}\left(t\right)}{m_d} + \frac{f_{d,KL}\left(t\right)}{m_d} \quad (9) $$

Then, $f_{z+1,NL}\left(t\right)$ is the nonlinear term of the restoring force of the $(z+1)$ floor, $a\left(t\right)$ is the ground acceleration and $\varepsilon_{dr}(t)$ represents the approximated dissipated energy (i.e. the sum of the dissipated and linear potential energy). The restoring force is approximated by $f_d\left(t\right) \cong -\left(a\left(t\right) + \ddot{u}_d\left(t\right)\right) m_d$. Then, β_d, γ_d and N_d are the conventional Bouc–Wen parameters, while δ_{dr} are the

degradation constants that multiply the dissipated energies. At this point, (6), (7, 8), (9), the system (5) and (3, 4) can be used to find the unknown parameters ${}^{d}p_i$. In this procedure, the parameters N_d are found by employing optimization algorithms that try to minimize the following cost function:

$$ {}^{d}J({}_{o}{}^{d}\boldsymbol{p}; N_d) = \int_0^{t_e} \left(\int_0^{f_s/2} {}^{d}W(f, \tau; {}_{o}{}^{d}\boldsymbol{p}) df \right) d\tau \qquad 10 $$

where for each trial value of N_d (starting from $d = D$ and proceeding in decreasing order), ${}_{o}{}^{d}\boldsymbol{p}$ can be easily found, and thus their values are known while calculating ${}^{d}J({}_{o}{}^{d}\boldsymbol{p}; N_d)$ from (10). A limitation of the method regards the mass matrix components, m_d, that should be known. If they are not known, it is necessary to estimate their values, e.g. values are obtained from calibrated Finite Element (FE) model of the structure.

After the identification of the model parameters, the values of ${}^{d}\boldsymbol{p}$ and N_d are known $\forall d$. Thus, it is possible to evaluate $K_{dr}(\varepsilon_{dr}(t), t) = K_{0,dr} \bullet (1 - \delta_{dr} \bullet \varepsilon_{dr}(t))$, where $K_{dr}(\varepsilon_{dr}(t), t)$ is the damaged stiffness linear stiffness matrix component, function of the approximated dissipated energy.

If the mass is assumed to remain almost constant after the occurrence of damage (and this is true in civil engineering structures, since a sensitive reduction in the mass occurs only in severe cases, where the detection of the damage can be easily performed by visual inspection), the following time-dependent eigen problem can be solved $\forall t$:

$$ \left(\mathbf{K}(t) - \omega_s^2(t) \bullet \mathbf{M} \right) \bullet \boldsymbol{\phi}_s(t) = 0 \qquad 11 $$

Thus, for each time instant, we can evaluate the damaged pulsations circular frequency of the system $\omega_s(t)$, and the damaged eigenvectors $\boldsymbol{\phi}_s(t)$ for each mode, s, in the chosen direction of the analysis. This provides the input for the evaluation of the instantaneous percentage of participation mass mass participation, $c_s(t)$:

$$ \boldsymbol{\Gamma}(t) = \boldsymbol{\phi}(t)^T \mathbf{M} \boldsymbol{v} \qquad 12 $$

13

$$c_s(t) = \frac{\Gamma_s^2(t)}{\sum_s \Gamma_s^2(t)}$$

where $\boldsymbol{v}$ is the a unitary drag vector, $\boldsymbol{\Gamma}(t)$ is the vector of the modal participation factors, and $\mathbf{M}$ is the mass matrix. Then, $c_s(t)$ can be used as a weighting factor for the damage index, $\iota(t)$, defined as follows:

$$\alpha_s(t) = 1 - \frac{\omega_s(t)}{\omega_s(0)} \quad (14)$$

$$\iota(t) := \boldsymbol{c}(t)^T \boldsymbol{\alpha}(t) \quad (15)$$

where $\alpha_s(t)$ is the normalized difference of the pulsation circular frequency for mode, s. The damage index defined in (14) depends only on by the mass of the system and ~~on~~ the variation of the stiffness linear term of the stiffness matrix during the seismic event. Table 1 reports a pseudo-code of the proposed algorithm, while Fig. 1 reports the corresponding flow-chart.

Table 1

Pseudo-code for the nonlinear identification of the seismic damage

Assume a direction of the seismic action, then:
A) Initialize $d = D$
a. Assume a value of N_d
i. Calculate the linear TFD of the quantities defined in (7, 8) and (9), then apply (3) (3) and (4) for ~~i~~*i* and ~~k~~*k* that go from 1 to ${}^dI$
ii. Solve the system of Eqs. (5) subjected to the desired constraints and/or boundaries
iii. Evaluate the cost function with (10)
b. Assume a new value of N_d and try to minimize (10) with a desired algorithm (following the steps i., ii. and iii.)
c. Find $N_d = {}_oN_d$ that minimize (10)
d. Find ${}_o^d p_i$ solving the system of Eq. (5) with $N_d = {}_oN_d$. Perform it in time or constant domain
B. Start the identification for another DoF
a. Update variable d as follow: $d = d–1$
b. Repeat the steps a., b., c. and d. of A) and a. of B) unless $d = 0$.

Assume a direction of the seismic action, then:
C. Evaluate the seismic damage
a. Evaluate the damaged stiffness matrix: $K_{dr}\left(\varepsilon_{dr}\left(t\right),t\right)=K_{0,dr}\left(1-\delta_{dr}\bullet\varepsilon_{dr}\left(t\right)\right)$
b. Solve the time-dependent eigen problem
c. Evaluate the instantaneous percentage of participation mass;
d. Evaluate the damage index $\iota\left(t\right)$ with (15)

Fig. 1

Flowchart of the pseudo-code

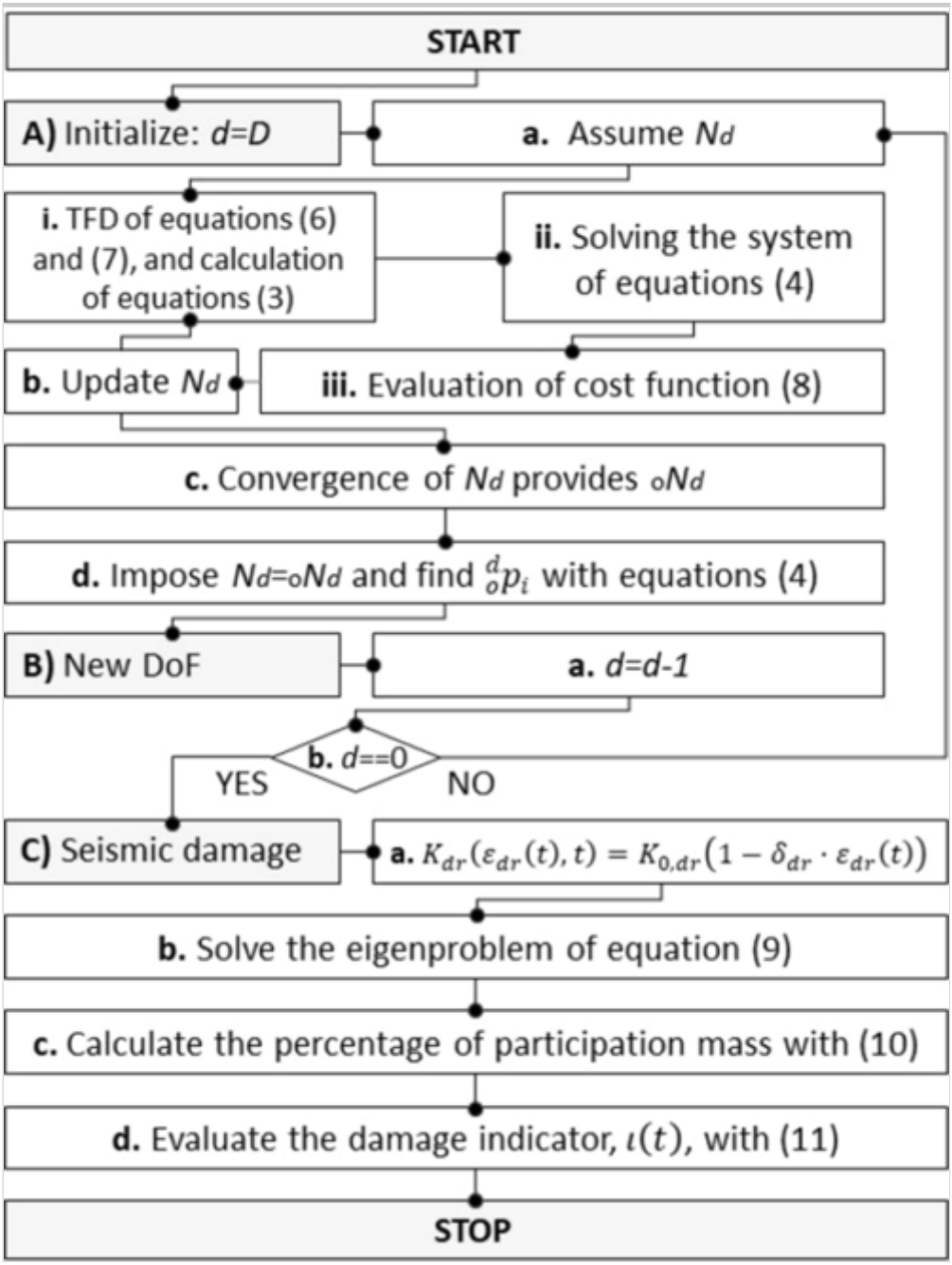

It is worth underlining that the described technique requires all relevant DoFs to be instrumented. In case of non-instrumented DoFs, one should appeal to nonlinear model reduction and expansion, which is an open issue that is out of the scope of this paper.

3. Application

In this section, the procedure described in Table 1 is applied to a monitored masonry structure, the Town Hall of Pizzoli (AQ) (Fig. 3a). The building is a two-storey stone-masonry building located northwest of the city of L'Aquila (Abruzzo), which is about 15 km away. The Town Hall was built around 1920 with a u-shaped plan mainly distributed along one direction, and its elevations are characterized by various regular openings. The building has three levels above the ground (the mezzanine floor, the first floor, the under-roof floor), and a basement. The total area is about 770 m^2, while the volume is about 5000 m^3. Previous investigations highlighted that the Town Hall presents a mixed masonry consisting of unsquared stone blocks, alternated with regular courses in solid bricks.

The building was affected by the seismic events that hit central Italy between 2016 and 2017 [27]. The permanent monitoring system installed on the building by the Seismic Observatory of Structures (OSS), allowed the recording of the seismic response of the structure and the seismic input (see Fig. 2), during the event of 30/10/2016.

Fig. 2

Seismic acceleration at the basement: **a** *X*-direction; and **b** *Y*-direction

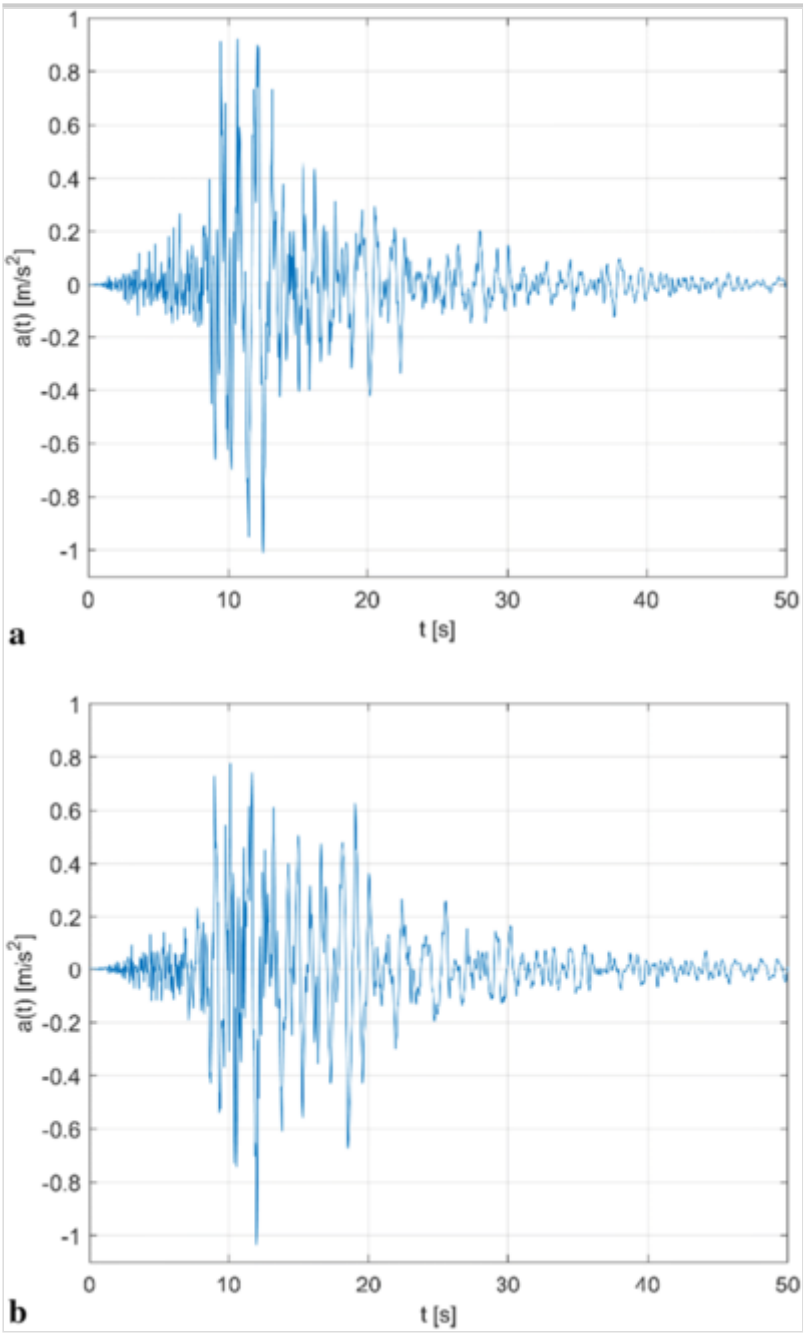

The records of channels 4, 10, 15 and 5, 11, 16 (see Fig. 3b for clarity) are the ones used for the detection of damage occurred during that event, since they are the most representative of the floor behaviour. A linear calibrated FE model of the system was available from a previous work [28] thus the masses of the floors (see Fig. 3c) were known in an approximated form.

Fig. 3

The Town Hall (**a**), the monitoring system (**b**), 2 lumped mass approximation (**c**)

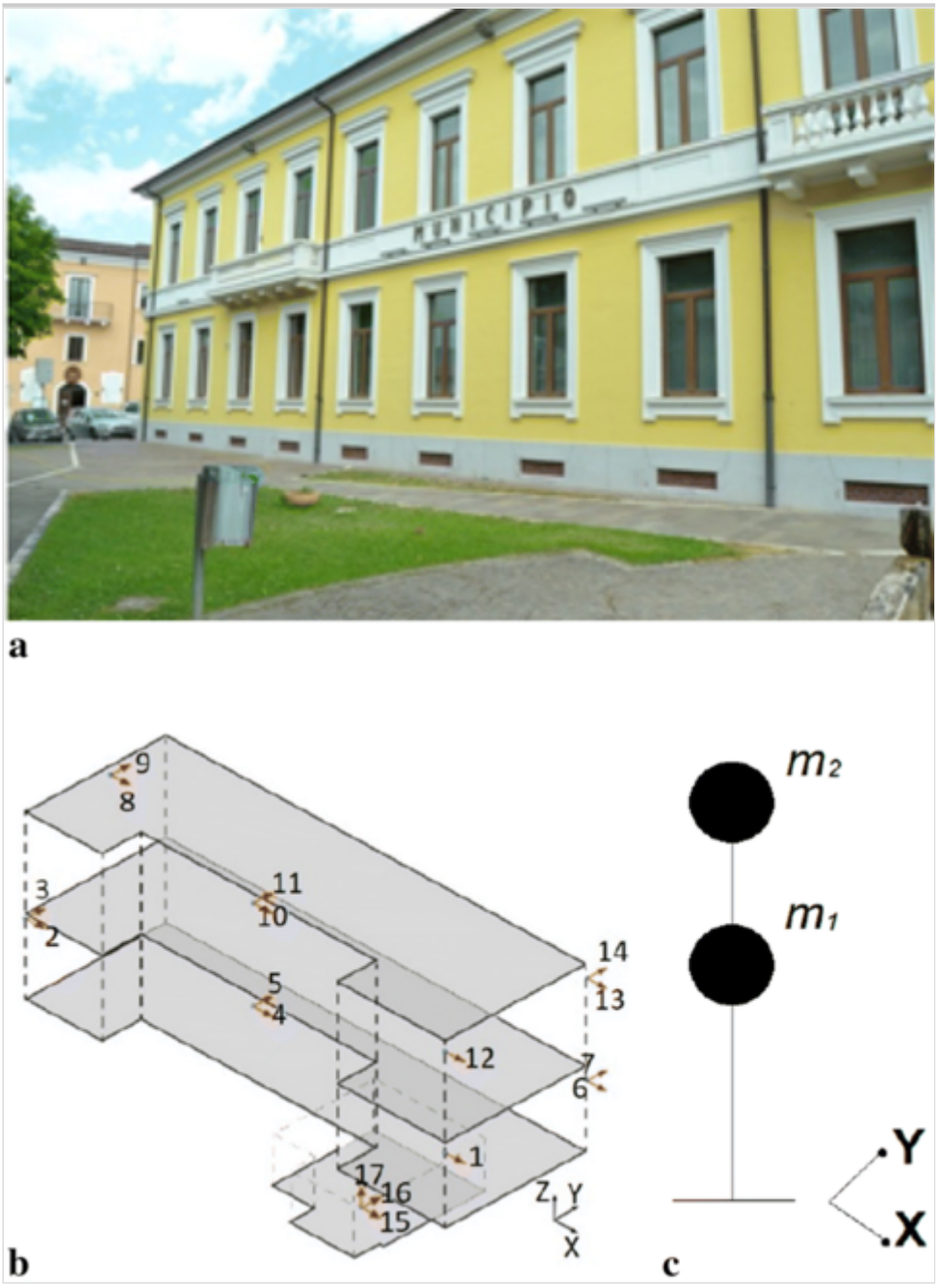

The procedure described in Table 1 has been applied with several algorithms (i.e. interior points, minimax, genetic, pattern search, simulated annealing, and particle swarm) to test the robustness of the identification. In addition, a finite set of solutions of ${}^{d}J(N_d)$ have been evaluated with a resolution of 0.001 on the values of N_d between 1 and 10. The chosen algorithms have been used to identify the nonlinear parameters of the Bouc–Wen model, N_d, for values that range between 1 and 10.

To get the displacement and the velocity responses, the raw accelerations data (sampled at 250 Hz for a useful length of about 50 s) were filtered with a band-pass Butterworth filter of order 4 with cut-off frequencies equal to 0.5 and 20 Hz.

The assumed TFDs were evaluated with a Short Time (Fast) Fourier Transform (SFFT) using a symmetric Hamming window. The length of the window was chosen to minimize the difference between the time points and frequency points of the TFD. This brought to a window of about 0.7920 s in length.

3.1. Nonlinear identification

To test the robustness of the methodology, the calibration was performed with six different optimization algorithms. All algorithms produced the same results, except for the interior point algorithm, that prematurely stuck into a local minimum. For brevity, Fig. 4 and Fig. 5 show the result in terms of β_2 and γ_2 as a function of time, while the numerical values estimated considering $t = t_e$ in (5) (the entire length of the signal) is reported at the top of the figures. The instantaneous estimation of the parameters allowed to check the stability of the results. Before reaching about 10 s, the values are unstable, because nonlinearity had not activated yet in the structure (Fig. 6).

Fig. 4

Instantaneous β_2 parameter: **a** *X*-direction; and **b** *Y*-direction

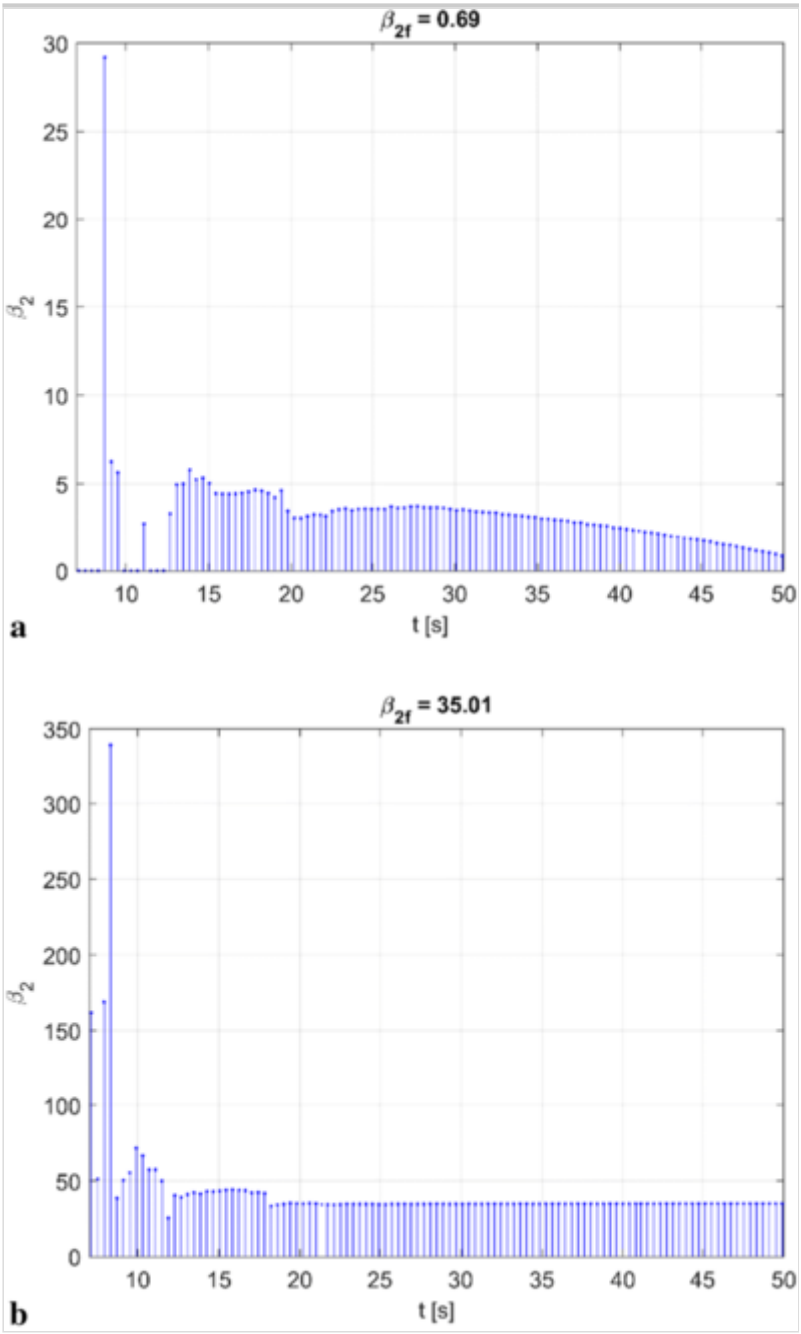

Fig. 5

Instantaneous γ_2 parameter: **a** *X*-direction; and **b** *Y*-direction

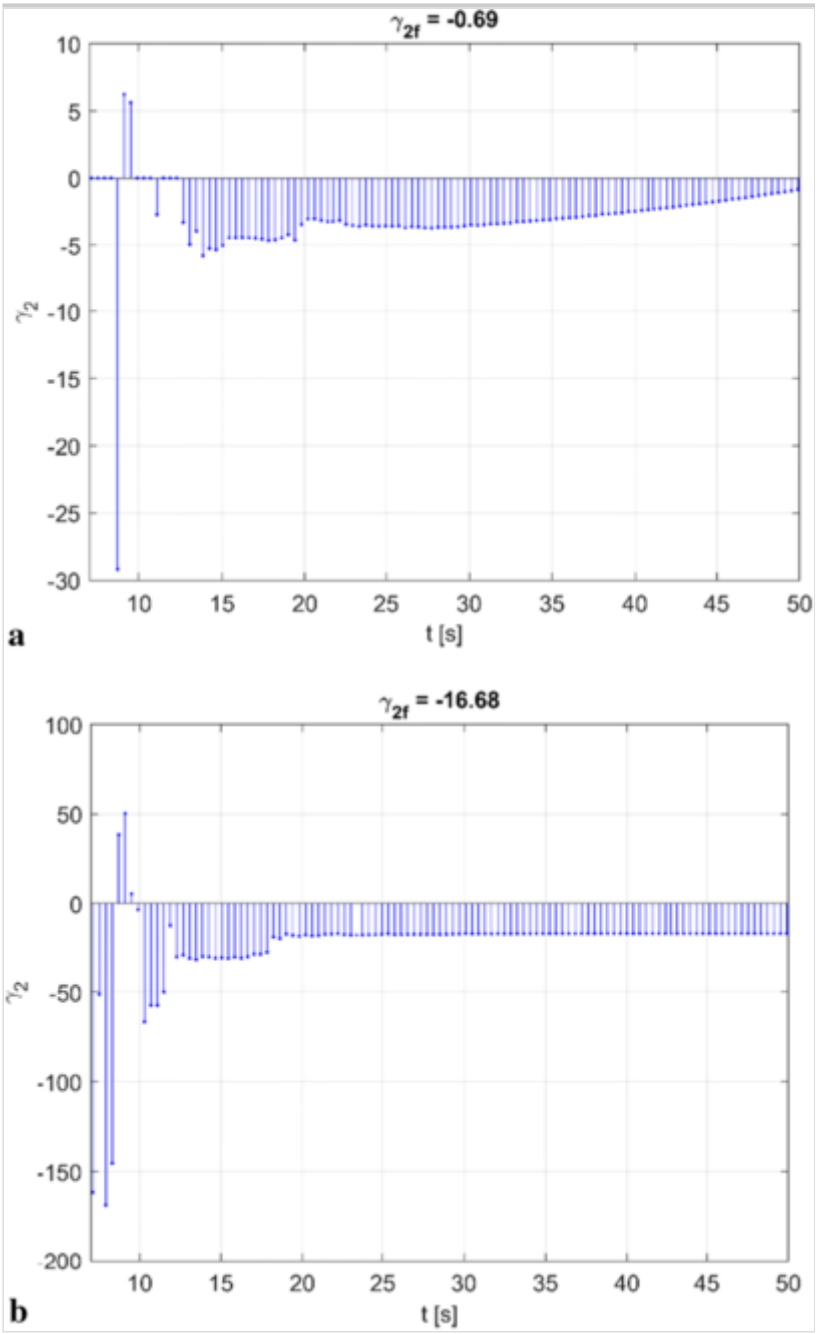

Fig. 6

Model fitting for the first DoF: **a** *X*-direction; and **b** *Y*-direction

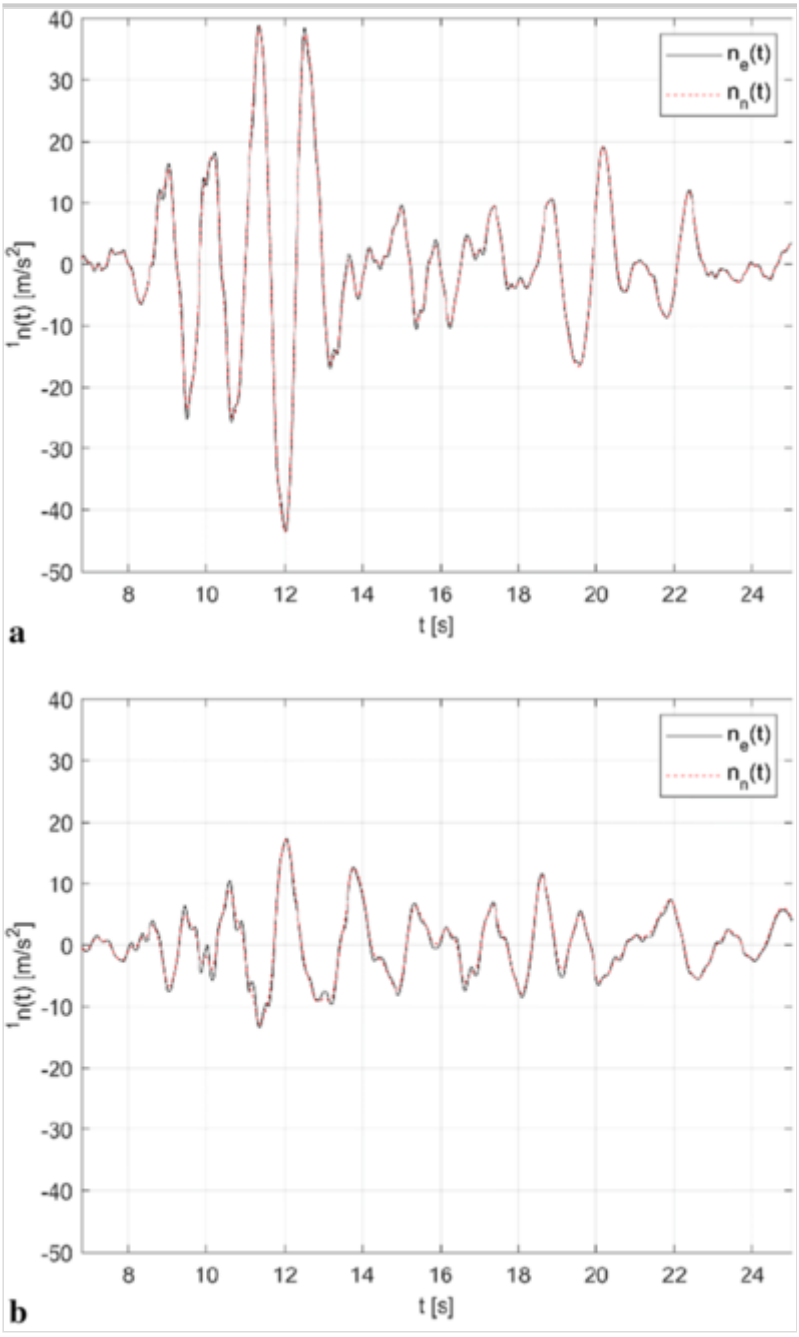

AQ2

This is an expected finding, as reported in [2], as the parameters associated to a nonlinear behaviour can reach stable values only in presence of significant nonlinearity levels (e.g. damage). This is also demonstrated by the greater stability of the parameters in the *Y*-direction, which, as will be shown, is associated to a greater damage with respect to the *X*-direction. For this reason, the stability along time of the parameters (e.g. statistical variance) can be also used to check the feasibility of the use of a nonlinear model with respect to another one (e.g. linear elastic, linear elastic with rate dependent capability, nonlinear model without hysteresis etc.). Figures Figs. 5 6 , 7 show the fitted data, $^{d}n_e(t)$, with the model described by $^{d}n_n(t)$ for both the *X*- and *Y*-direction. From these figures, it is possible to notice that the model replicates in an acceptable way the data provided. Cleary, this does not demonstrate the

goodness of the model in reproducing the dynamics of the system subjected to other actions. However, this topic is beyond the scope of the proposed study, which instead focuses on the analysis of the damage caused by the specific recorded seismic action.

Fig. 7

Model fitting for the second DoF: **a** *X*-direction; and **b** *Y*-direction

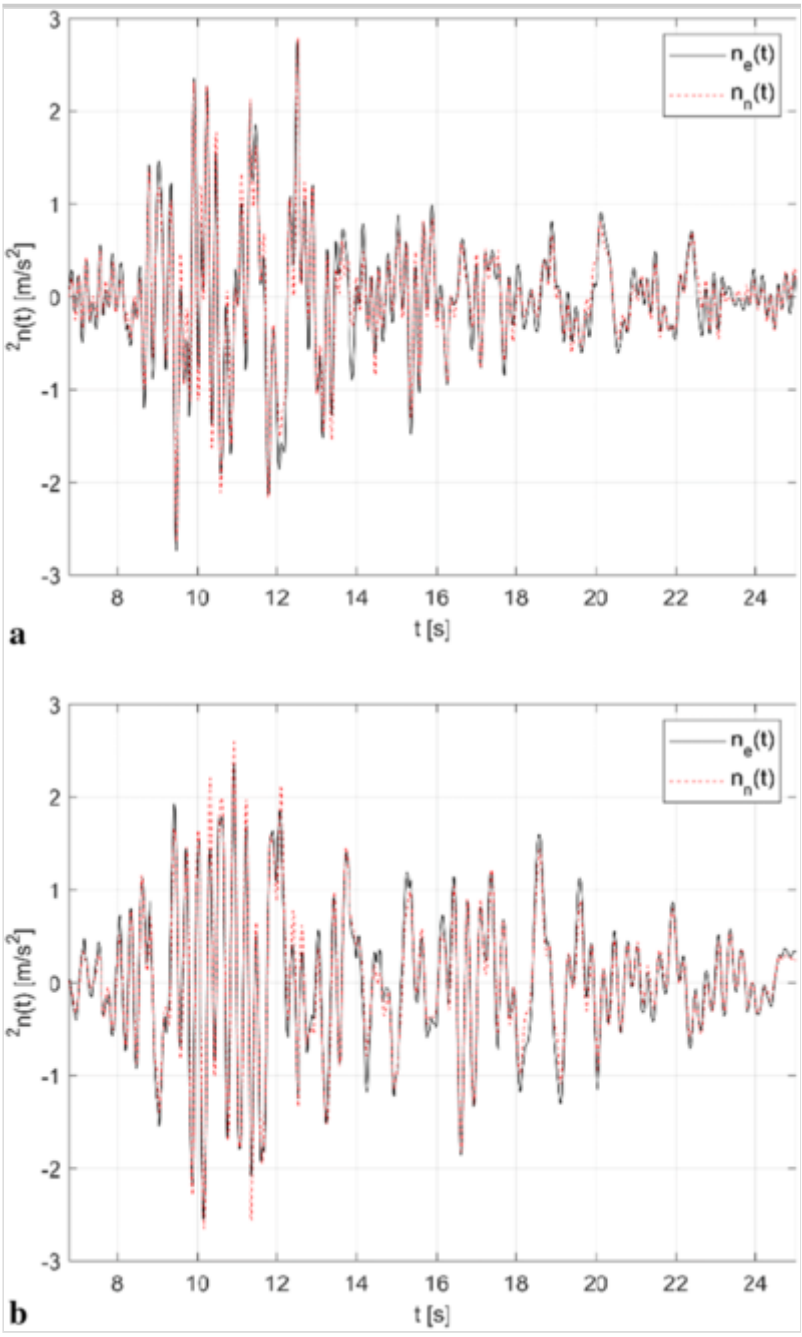

In Fig. 8, the TFDs of the structural response in terms of accelerations has been compared between the experimental records and the response obtained from the identified numerical 2 DoFs model (the average values of the time-varying parameters have been used for this purpose). The comparison shows a good

agreement between the localization in time of the frequency content predicted by the model and that one expected analysing the experimental data.

Fig. 8

Contour plot of the TFDs of the experimental (exp) and numerical (num) structural acceleration of the 2nd DoF: **a** *X*-direction; and **b** *Y*-direction

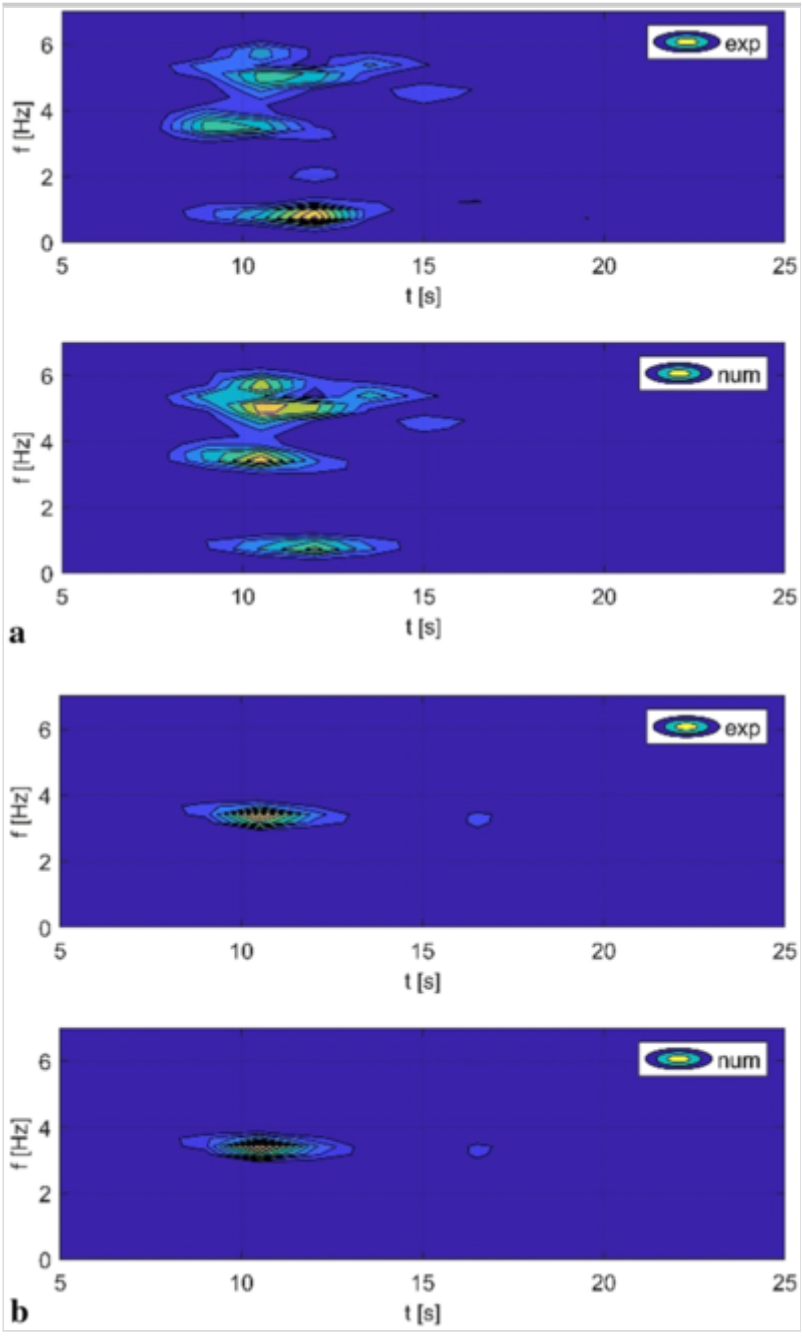

3.2. Damage detection

Following the calibration of the model, the time-dependent eigen problem was solved to find the instantaneous frequencies and modal shapes.

These were used to calculate the damage index defined in (14) (15) and reported in Fig. 9.

Fig. 9

Damage index: **a** *X*-direction; and **b** *Y*-direction

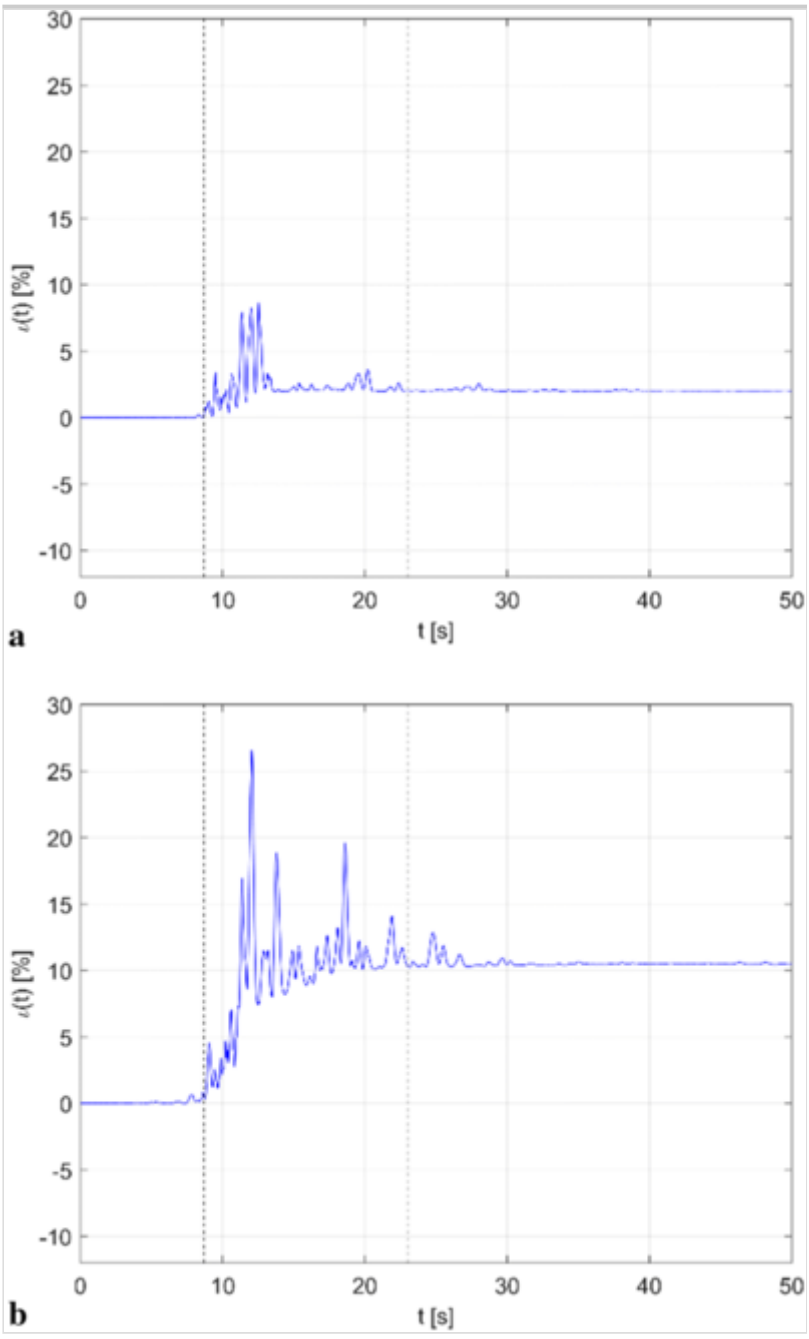

From the figure, it is possible to see that the damage index reaches a stabilization after passing the moments of maximum amplitude of the quake. After the stabilization phase, the value of $\iota(t)$ cannot decrease. The damage index at the end of the analysis can be thus accepted as an estimation of the damage occurred during the seismic event, providing timely information on the health state of the structure.

As regards to the case study, following the assumed model, the main damage was detected in the *Y*-direction (along the short dimension of the building) and the value of the damage index is about 10%. In the *X*-direction (long dimension of the building), instead, the damage was more contained, approaching values of 2%. It is worth mentioning that, since the dissipated energy has been approximated by the sum of the dissipated and elastic potential energy, during the quake, the damage index oscillates in accordance with this energy component, which is released (the damage index increases) and adsorbed (the damage index decreases) during the cycles. However, because the elastic potential energy is conservative, its value is zero at the beginning and at the end of the quake, thus the final estimate of the damage index is not affected by this energy term.

The occurrence of an increase of the damage index is a direct consequence of the change in the values of the time-varying frequencies estimated by solving the system (11), which in turn depends on the degradation of the linear stiffness terms, $K_{dr}\left(\varepsilon_{dr}\left(t\right),t\right)$, of the assumed Bouc–Wen model of hysteresis. It is also worth mentioning that small changes in modal quantities, and thus in the damage index, can be easily related to deviations in the stiffness matrix through well-known linearized formulations [29]. Thus, by excluding any mass changes, the damage index is related to a variation of stiffness by:

$$\iota\left(t\right)=1-\sum_{s}\left(c_{s}\left(t\right)\sqrt{\frac{\boldsymbol{\phi}_{s}{}^{T}(t)\mathbf{K}\left(t\right)\boldsymbol{\phi}_{s}(t)}{\boldsymbol{\phi}_{s}{}^{T}(0)\mathbf{K}\left(0\right)\boldsymbol{\phi}_{s}(0)}}\right) \quad 16$$

AQ3

In Fig. 10, the instantaneous estimates of the diagonal terms of the linear elastic stiffness matrix is reported for both directions of the seismic action. From the figure, one can easily recognize a general reduction of the initial values of the stiffness, except for K_{11} in *X*-direction.

Fig. 10

Time variation of the diagonal terms of the linear elastic stiffness matrix: **a** *X*-direction; and **b** *Y*-direction

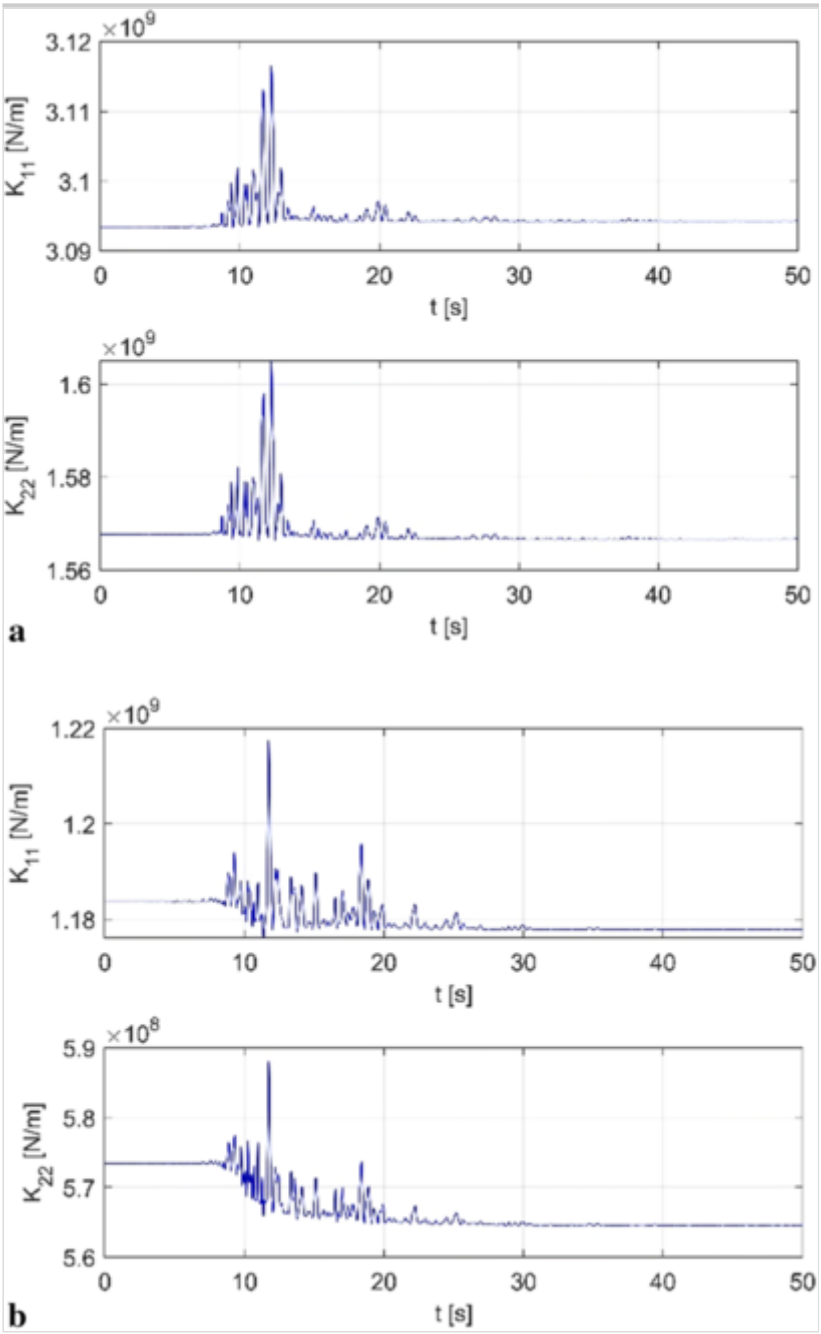

The value estimated for this term, at the end of the quake, resulted to be very close to the value identified at the beginning, except for small errors due to the low values of the dissipated energy. In fact, for this term, the cumulated energy obtained by integration resulted very close to zero but negative in sign. This is due to small nonlinear trends in the input signal, which are difficult to remove completely.

As regards to the remaining terms, it is possible to observe a reduction in the stiffness that is visibly higher in *Y*-direction than in *X*-direction. Comparing the absolute values of the stiffness terms it is possible to notice that the stiffness in *X*-direction is considerably higher than in *Y*-direction, with ratios that range from 2.6 for the first component to 2.7 of the second component. Instead, the ratio between K_{11} and K_{22} is approximately 1.97 in *X*-direction and 2.06 in *Y*-

direction. Recalling a shear-type model, this means that the total stiffness of the first floor equals the total stiffness of the second floor.

The stiffness degradation reflects in a reduction of natural frequencies. In Fig. 11, the two frequencies obtained solving the eigen problem (11) at each time [25] are reported for each direction of the building. For the natural frequencies one can observe that the reduction is detected for each mode except for the second one in *X*-direction, for which an increase of about 0.16‰ in frequency is estimated. As regards to the other modes, the ratio between the natural frequencies after and before the quake resulted to be 0.977 for the first mode in *X*-direction and 0.998 and 0.892 for the second and first mode in *Y*-direction, respectively. Comparing the absolute values of the frequencies it is possible to notice that the values in *X*-direction are quite higher than those one in *Y*-direction, with a ratio that ranges from 1.07 for the first mode to 1.66 of the second mode.

Fig. 11

Time variation of the natural frequencies: **a** *X*-direction; and **b** *Y*-direction

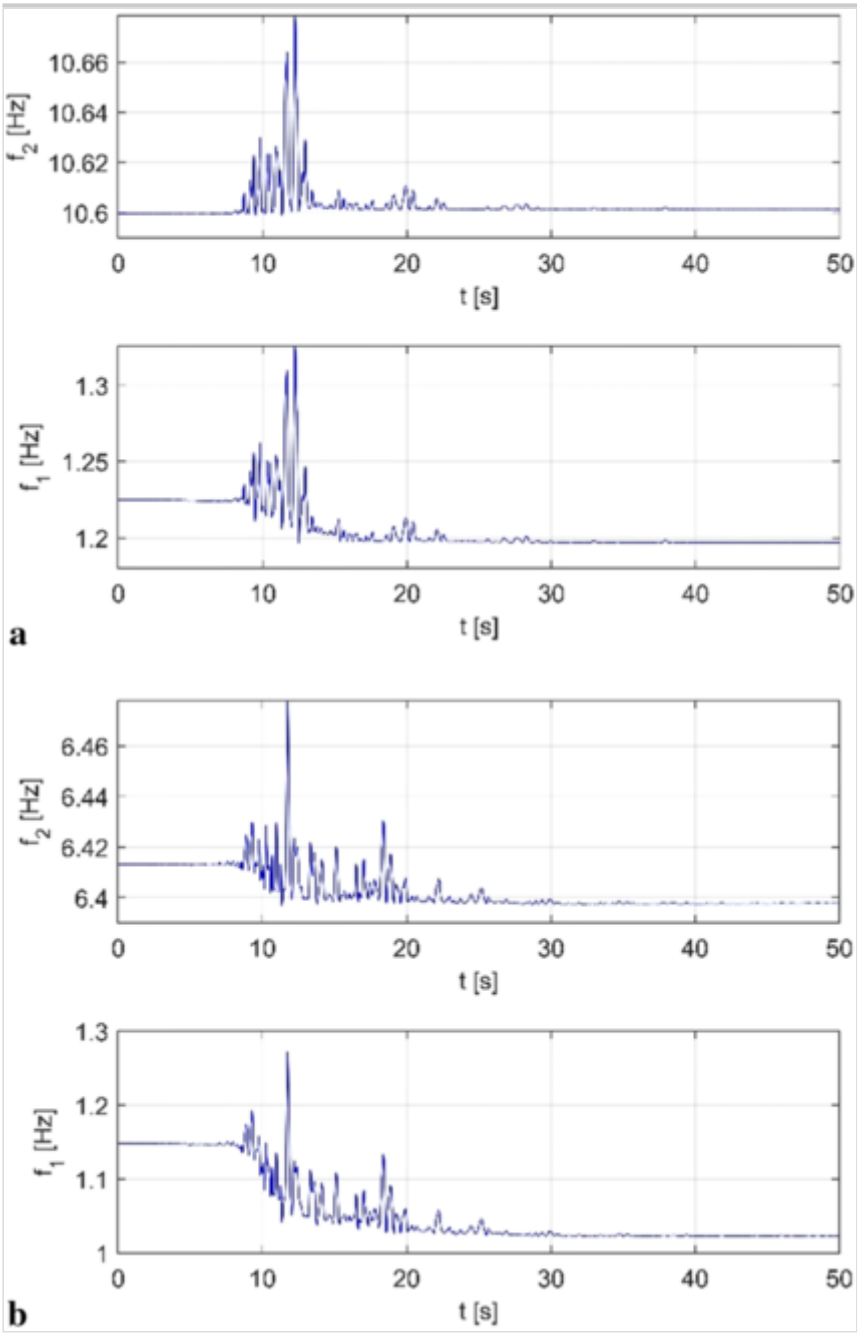

The considerations made for natural frequencies do not applies to mode shapes. From Fig. 12 it is clear that the correlation between the eigenvectors before and after the quake is very high for both directions. This is commonly related to the presence of low damage uniformly distributed along each direction of the building. The percentage of mass participation remains almost constant and equal to about 97.5% for the first mode and 2.5% for the second mode in both directions.

Fig. 12

Mode shape before and after the main shock: **a** *X*-direction; and **b** *Y*-direction

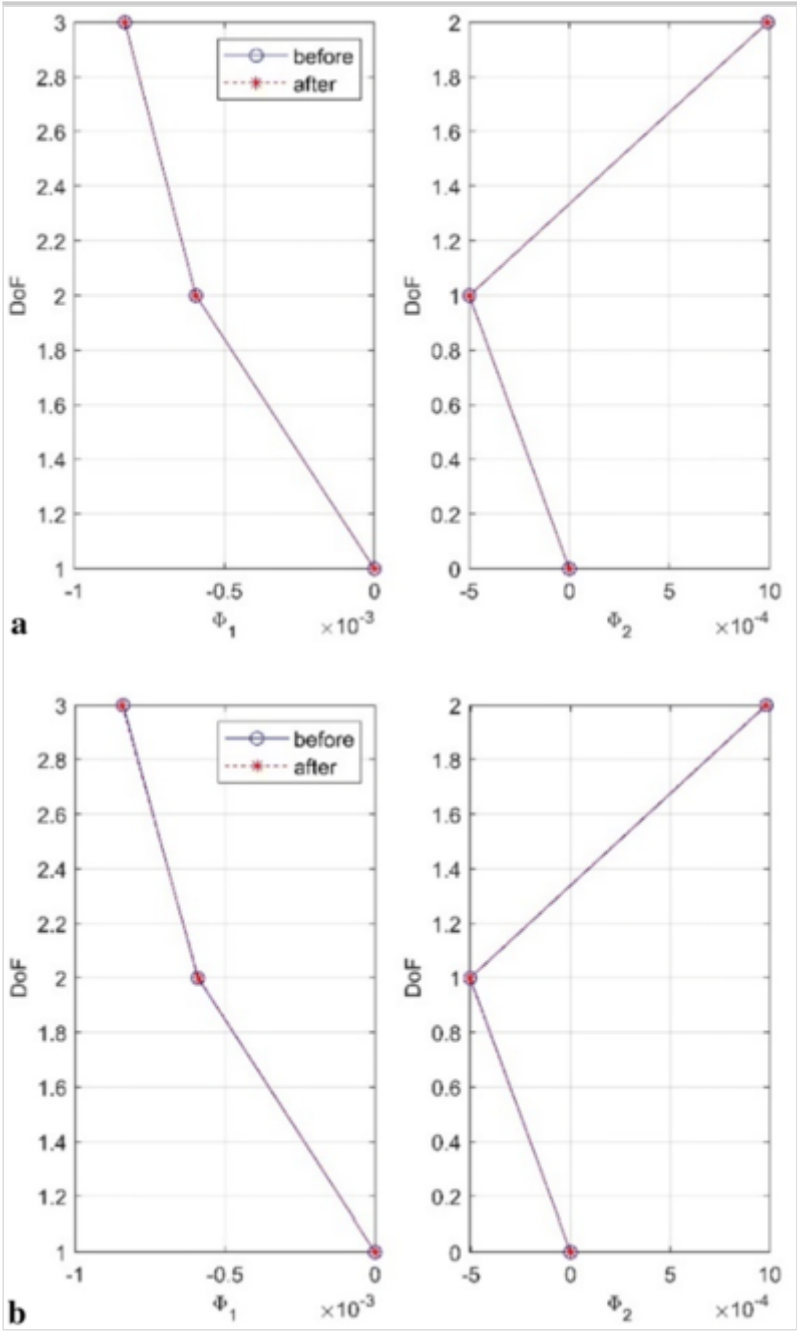

~~From Eq. (12),~~ for For values of the damage index lower than 5% the average stiffness reduction is less than 10%. In the latter this case, damage detection will need to account for parameter wandering, e.g. due to environmental fluctuations.

More generally, at least for small changes of modal parameters, Eq. (12) (15) can directly relate the proposed damage index to inter-storey stiffness reductions in buildings. In case of important changes in the modal parameters, damage indexes need to comply with the standards used in post-seismic damage inspection for different building types. Based on damage severity, for different building types, standards and guidelines also provide indications on the levels of precaution to be undertaken on a building immediately after a seismic event [30].

4. Verification of the methods

In this section, some verifications of the damage detection procedure are performed to support the analysis. In this respect, the inter-storey drift, $\Delta \boldsymbol{u}(t)$, in the two directions of the building are reported in Fig. 13. These are substantially consistent with the numerical estimates reported in, Fig. 9. In fact, Fig. 13 shows that, despite the inter-floor drift peak being approximately the same in the two directions, in *Y*-direction high values of drift are maintained for a longer time. Comparing Figs. 13, 9, it is also possible to note that as soon as the inter-storey drift increases in amplitude, the system starts to develop damage in accordance with the adopted model. The energy loss is then represented by an alteration of the stiffness values, and thus in an alteration of the natural frequencies.

Fig. 13

Inter-floor drift of the first and second floor: **a** *X*-direction; and **b** *Y*-direction

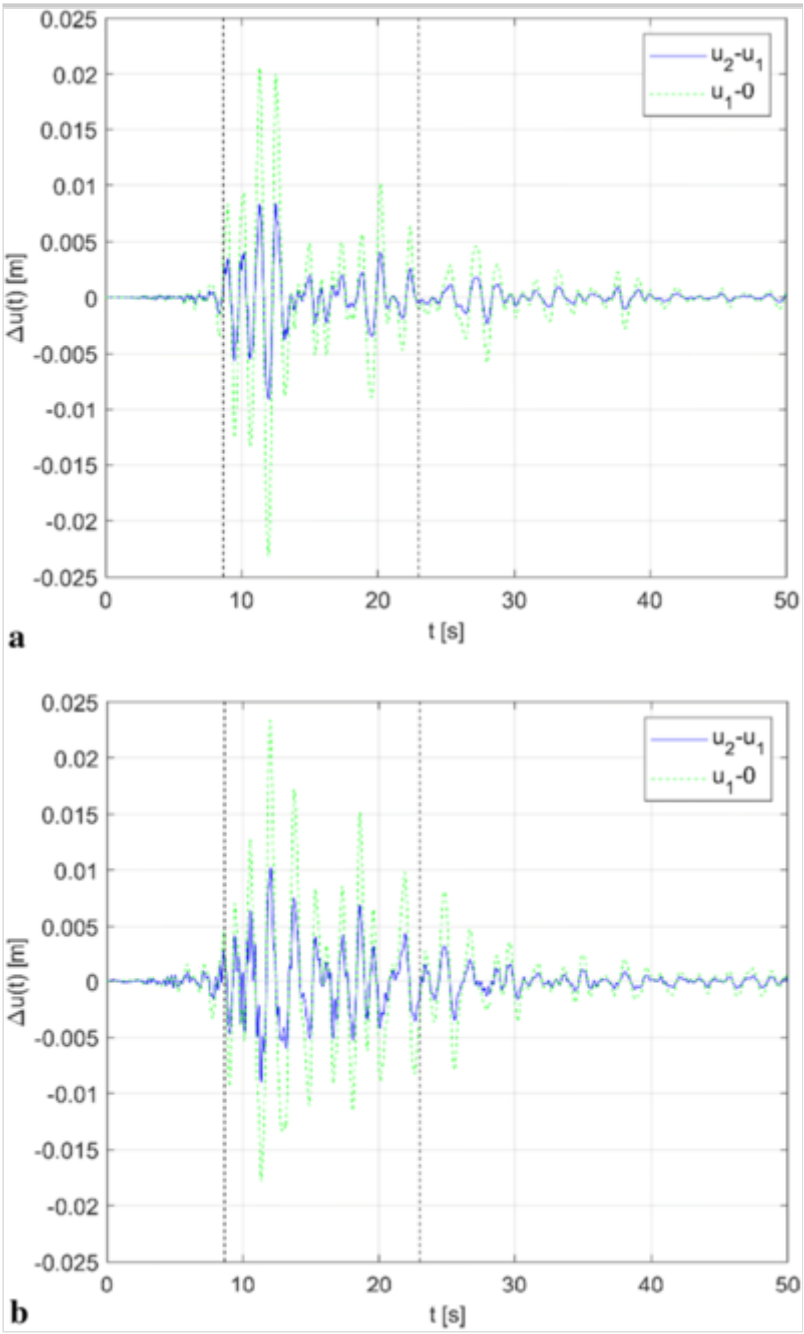

Figure Fig. 14 documents the damage observed after the seismic sequence that struck Central Italy in 2016 and 2017 [31]. The original report specifies that the building did not show local mechanisms, but rather the effects of a global response. The inspection highlighted a mild pattern of through cracks in most masonry walls along *Y*-direction. In *X*-direction, instead, only a widespread pattern of superficial cracks was observed [32]. These findings are consistent with the results of the nonlinear identification in terms of damage, as inferred from Fig. 9.

Fig. 14

Damage observed on the Pizzoli town hall: **a** and **b** damage on prospect 2 (P2) and 5 (P5) after the seismic sequence of 2016–2017, [31, 32]; **c** pseudo-vertical crack in Room n. 02 at 1st floor (RI02), and; **d** raised ground floor plan

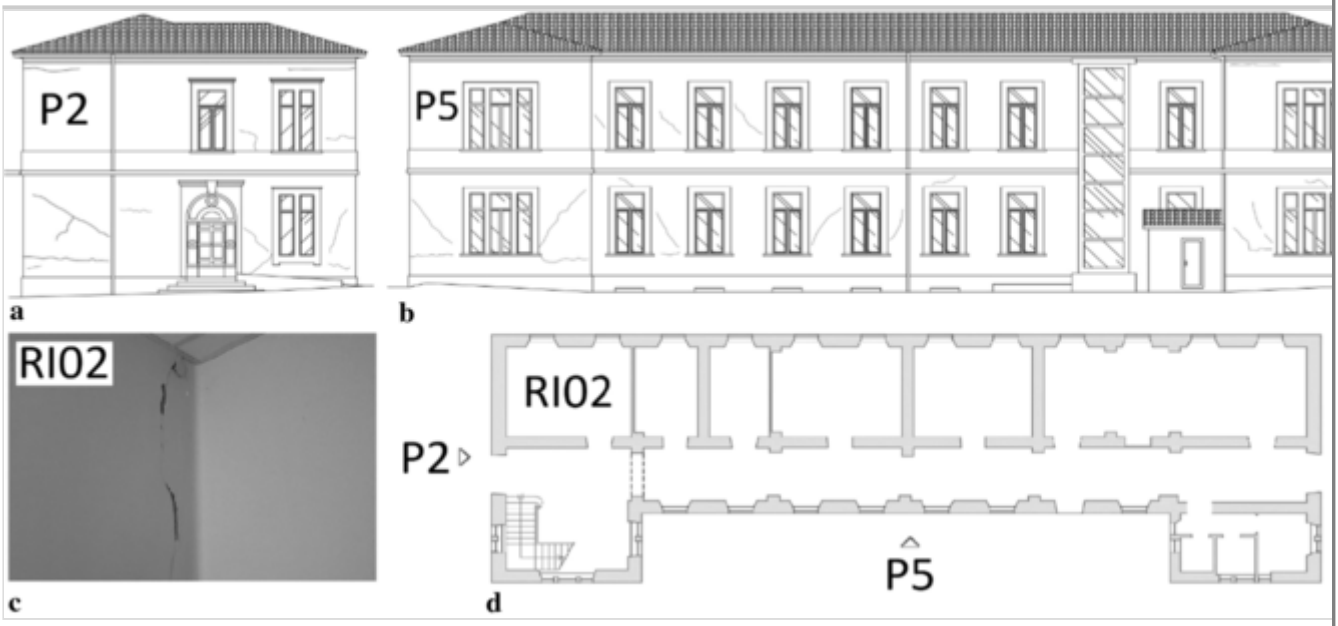

AQ4

To further check the results of the identification, the Zero Crossing Rate (ZCR) [33] of the building's response before and after the main shock was then calculated for the two directions of the building. Given the unavailability of ambient vibration records after the main shock of 30 October 2016, the signals recorded during the minor events of 07 September 2016 and 03 November 2016 were used for the ZCR plots of Fig. 15. The ZCR was evaluated from free response segments (i.e. when sensible effects of the input tend to disappear) as reported in Fig. 15. Comparing the values calculated before and after the main shock, an average reduction in the ZCR of 13% has been estimated. It is worth mentioning that between 07 September 2016 and the main shock two other earthquakes were registered. However, the building was mainly damaged by the event of 30 October 2016 and the following one of January 2017.

Fig. 15

Free vibration response to minor events in terms of displacements and ZCR before and after the main shock: **a** *X*-direction; and **b** *ss*-direction

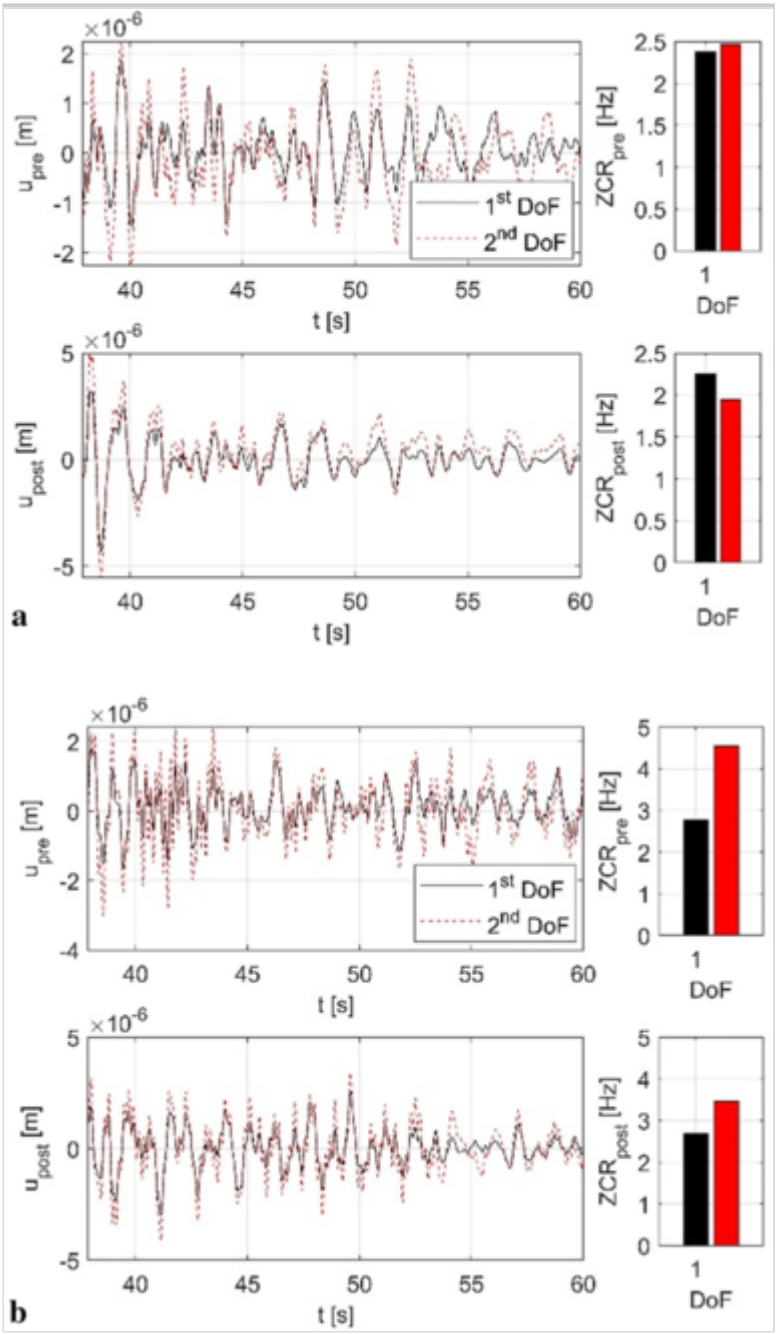

5. Conclusions

In this paper, the seismic damage occurred in a monitored masonry building has been identified by fitting the structural response with a hysteretic Bouc–Wen-type law. This allowed the definition of floor laws and corresponding damage indices~~ex~~ for each direction of the seismic action. The method described consists of three main steps:

i. Calculation of the TFD of the records and instantaneous identification of the model parameters;

ii. Consistency checks on the identification results, and;

iii. Estimation of the damage induced by the seismic event.

It is worth mentioning that the mechanical nonlinearity of materials is not the only complex behaviour that is encountered when working with masonry structures, especially historical buildings. Other complex behaviors can arise from heterogeneity of construction, e.g. a poor connection between the subparts of systems (wall–wall, floor–wall, etc.). In fact, the presence of disconnections can affect the observed dynamic response and may corrupt the identification processes if the mathematical models are not able to represent them. In the paper, the latter behaviors have not been considered, therefore, in principle, uncertainties remain in the calibration results.

For the specific case of the Town Hall of Pizzoli, a global box-like behaviour was assumed, also based on the results of on-site inspections that led to the verification of the existence of good connections between walls and floor–walls, before the occurrence of the seismic events. The main results are summarized in the following points:

i. The basis functions to estimate the model parameters of a simple Bouc–Wen-type oscillator have been derived for chain-like~~?~~ MDoF systems;

ii. The adopted procedure allowed to verify the consistency of the assumed nonlinear model. This has been done by checking the stability of the values of the model parameters in ~~the~~ time;

iii. The resulting model satisfactorily reproduces the experimental response;

iv. The procedure is very efficient (a couple of seconds of analysis are needed), allowing timely information on the health of the structure immediately after the occurrence of the earthquake, so helping to manage decision-making processes for post-seismic scenarios.

A possible drawback of the study is represented by the fact that currently the procedure cannot be applied to general MDoF systems because of the assumption of independent behaviour in the two directions and of a chain-like hysteretic inter-storey law. Thus, an extension is needed. Moreover, the method can be only applied if all the relevant DoFs of the building are instrumented. Otherwise, the identification process should possibly rely to nonlinear reduction / expansion techniques or other specialized tools that are out of the scopes of this study.

As regards to the definition of a damage index, at least in principle, only its final value is representative of the actual damage state. A possible solution to improve

the significance of instantaneous damage estimates can consist in removing higher frequency components, that are associated to the conservative term.

An improvement of the identification procedure might consist in assigning appropriate probabilistic distributions for the parameters, and introducing discrepancy functions to check how closely the identified nonlinear model conforms to the observed data. This would be useful for detecting low damage levels, especially in the presence of noise and errors that tend to propagate in the process.

Publisher's Note

Springer Nature remains neutral with regard to jurisdictional claims in published maps and institutional affiliations.

Acknowledgements

The research was partially funded by Compagnia di San Paolo, within the project: “System Identification, model updating and damage assessment of heritage buildings and structures”. The data of the Town Hall of Pizzoli were supplied by the Seismic Observatory of Structures within the DPC-ReLUIS project.

References

1. Loh CH, Lin CY, Huang CC (2000) Time domain identification of frames under earthquake loadings. J Eng Mech 126(7):693–703

2. Ceravolo R, Erlicher S, Zanotti Fragonara L (2013) Comparison of restoring force models for the identification of structures with hysteresis and degradation. J Sound Vib. 332:6982–6999

3. Sireteanu T, Giuclea M, Mitu AM (2010) Identification of an extended Bouc-Wen model with application to seismic protection through hysteretic devices. Comput Mech 45(5):431–441

4. Wang Z, Lin RM, Lim MK (1997) Structural damage detection using measured FRF data. Comput Methods Appl Mech Eng 147(1–2):187–197

5. Cappello C (2017) Theory of decision based on structural health monitoring, Trento: Doctoral dissertation, University of Trento

6. Asteris PG, Chronopoulos MP, Chrysostomou CZ, Varum H, Plevris V, Kyriakides N, Silva V (2014) Seismic vulnerability assessment of historical masonry structural systems. Eng Struct 62:118–134

7. Hale JE, Dulek RE, Hale DP (2005) Crisis response communication challenges: building theory from qualitative data. J Bus Commun 42(2):112–134

8. Farrar CR, Worden K (2012) Structural health monitoring: a machine learning perspective. Wiley, Hoboken

9. Bouc R (1971) Mode` le mathe´matique d'hyste´re´sis. Acustica 24:16–25

10. Wen Y (1976) Method for random vibration of hysteretic systems. J Eng Mech Div ASCE 102:249–263

11. Baber T, Wen Y (1981) Random vibrations of hysteretic, degrading systems. J Eng Mech Div ASCE 107:1069–1087

12. Ikhouane F, Rodellar J (2005) On the hysteretic Bouc-Wen model. Nonlinear Dyn 78:42–63

13. Chassiakos A, Masri S, Smyth A, Anderson J (1995) Adaptive methods for the identification of hysteretic structures, Proceedings of the American control conference, p. 2349–2353

14. Smyth A, Masri S, Kosmatopoulos E, Chassiakos A, Caughey T (2002) Development of adaptive modelling techniques for non-linear hysteretic systems. Int J Nonlinear Mech 37:1435–1451

15. Ashrafi S, Smyth A (2008) Adaptive parametric identification scheme for a class of nondeteriorating and deteriorating nonlinear hysteretic behavior. J Eng Mach 134:482–494

16. Masri S, Caffrey J, Caughey T, Smyth A, Chassiakos A (2004) Identification of the state equation in complex non-linear systems. Int J Nonlinear Mech 39:1111–1127

17. Benedettini F, Capecchi D, Vestroni F (1995) Identification of hysteretic oscillators under earthquake loading by nonparametric models. J Eng Mech 121:606–612

18. Pei J, Smyth A, Kosmatopoulos E (2004) Analysis and modification of Volterra/Wiener neural networks for the adaptive identification of non-linear hysteretic dynamic systems. J Sound Vib 275:693–718

19. Brunton S, Proctor J, Kutz J (2016) Discovering governing equations from data by sparse identification of nonlinear dynamical systems. Proc Nat Acad Sci 113(15):3932–3937

20. Lai Z, Nagarajaiah S (2019) Sparse structural system identification method for nonlinear dynamic systems with hysteresis/inelastic behavior. Mech Syst Signal Process 117:813–842

21. Carboni B, Lacarbonara W, Brewick PT, Masri SF (2018) Dynamical response identification of a class of nonlinear hysteretic systems. J Intell Mater Syst Struct 29(13):2795–2810

22. Noël J, Kerschen G (2017) Nonlinear system identification in structural dynamics: 10 more years of progress. Mech Syst Signal Process 83:2–35

23. Ceravolo R, Demarie G, Erlicher S (2010) Instantaneous identification of degrading hysteretic oscillators under earthquake excitation. Struct Health Monit 9:447–464

24. Pai P, Huang L, Hu J, Langewisch D (2008) Time-frequency method for nonlinear system identification and damage detection. Struct Health Monit 7:103–127

25. Bursi O, Ceravolo R, Erlicher S, Zanotti LF (2012) Identification of the hysteretic behaviour of a partial-strength steel–concrete moment-resisting frame structure subject to pseudodynamic tests. Earthq Eng Struct Dyn. 41(14):1883–1903

26. Asgarieh E, Moaveni B, Barbosa AR, Chatzi E (2017) Nonlinear model calibration of a shear wall building using time and frequency data features. Mech Syst Signal Process 85:236–251

27. Ceravolo R, Lenticchia E, Miraglia G (2019) Spectral entropy of acceleration data for damage detection in masonry buildings affected by seismic sequences. Constr Build Mater 210:525–539

28. Miraglia G, Lenticchia E, Ceravolo R, Betti R (2019) Synergistic and combinatorial optimization of finite element models for monitored buildings.

Struct Control Health Monit 26(9):e2403

29. Fox RL, Kapoor MP (1968) Rates of change of eigenvalues and eigenvectors. AIAA J 6(12):2426–2429

30. Di Ludovico M et al. (2019) Usability and damage assessment of public buildings and churches after the 2016 Central Italy earthquake: The ReLUIS experience," in In 7th International Conference Earthquake Geotechnical Engineering for Protection and Development of Environment and Constructions, Rome

31. Cattari S et al.(2019a) Discussion on data recorded by the Italian structural seismic monitoring network on three masonry structures hit by the 2016–2017 Central Italy earthquake
AQ5

32. Cattari S et al. (2019b) WP4_4.1: report di sintesi sulle attività svolte sugli edifici monitorati dall'Osservatorio Sismico delle Strutture e danneggiati durante la sequenza sismica del Centro Italia 2016–2017," Università degli Studi di Genova, Università degli Studi di Chieti-Pescara, Università degli Studi di Pavia, Università di Padova, ITC Padova, Politecnico di Torino, Osservatorio Sismico delle Strutture, (In Italian)

33. Dutta PK, Mishra OP (2017) Analysis of zero-crossing frequency and likelihood function for retrieval of maximum displacement in real time earthquake signal. Acta Technica 62(2):1–16